Bioinspiration & Biomimetics

PAPER

Bending, twisting and flapping leaf upon raindrop impact

RECEIVED
2 August 2019

REVISED
21 December 2019

ACCEPTED FOR PUBLICATION
7 January 2020

PUBLISHED
5 March 2020

Yashraj Bhosale[1], Ehsan Esmaili[2], Kinjal Bhar[2] and Sunghwan Jung[2]

[1] Department of Mechanical Science and Engineering, University of Illinois at Urbana Champaign, IL 61801, United States of America
[2] Department of Biological and Environmental Engineering, Cornell University, NY 14853, United States of America

E-mail: sunnyjsh@cornell.edu

Keywords: drop impact, leaf, bending

Supplementary material for this article is available online

Abstract

Dynamics of drop impact on soft surfaces has drawn a lot of attention for its applications and is motivated by natural examples like raindrop impact on a leaf. Previous studies have focused on categorizing the bending motion observed, using cantilever beam theory, but the complex dynamic response shown by a leaf involving other degrees of motions like torsion about the petiole, remains yet to be understood. In this study, we demonstrated that the complex response of a superhydrophobic Katsura leaf upon raindrop impact can be decomposed into simple single degree-of-freedom linear modes of bending and torsion, modeled as damped harmonic oscillators. Our theoretical estimates were in good agreement with experimental measurements of the frequency and maximum amplitude of bending and torsional modes. We also illustrated the energy transfer from the raindrop to these modes as a function of the impact location, which may shed light on the design of potential raindrop energy harvesting devices mimicking a leaf's structure. Finally, we concluded with a brief description of an unresolved mode (i.e. flapping) and the limitations of our approach.

Introduction

Typically, a leaf (shown in figure 1(a)) consists of a petiole and a lamina. The petiole is a thin supportive structure which connects and transports nutrients between the lamina and the stem. The lamina has commonly a flat blade-like structure functioning as the major photosynthetic energy harvester. Due to the flatness of the lamina, the leaf keeps moving in various ways in response to external forces: e.g. wind, animal touches, and raindrops [1–6]. The flattened structure of the lamina is a result of years of evolution for maximizing sunlight absorption and achieving structural stability in response to all these external factors [7, 8].

Similar to structural properties, material properties like surface hydrophobicity for leaves have been well exploited as an evolutionary survival strategy by plants [9]. The origin of this property is usually a chemical coating (cuticular wax) or surface roughness on the micrometer scale or a combination of both [10–12]. Hydrophobicity in the case of leaves may have many adaptive advantages. For example, hydrophobicity of a leaf surface leads to water drops rolling and accumulating into a bigger drop eventually rolling off while carrying the contaminants with them, thus keeping the leaf surface clean [9, 13]; known widely as the Lotus effect [14]. Recently, for leaves a change in wettability has been characterized over seasons [15] and temperature [16].

Unlike the scenario of a drop rolling off governed by surface hydrophobicity effects, in nature a falling raindrop impacts a hydrophobic leaf at high terminal velocities [17], and can lead to a completely different dynamic response of the system. The force of an impacting raindrop was measured by Soto *et al* [17] using a piezoelectric sensor and its peak force was found to be 500–1000 times that of the drop's weight. Such high impact forces can be severe and detrimental to roofs causing damage, soil causing erosion and plant leaves leading to a fall-off from a tree. With this as an inspiration, simple cantilever models have been used to explain the dynamic response of a slender quasi 1D leaf and the effects of surface wettability have been studied with regards to the forces experienced by the leaf [18, 19]. The relative extent of the two degrees of freedom, bending and torsion, experienced by the leaf petiole can be correlated to the ratios of bending and torsional rigidity which has been studied as a function of the structural and material properties of a leaf [20]

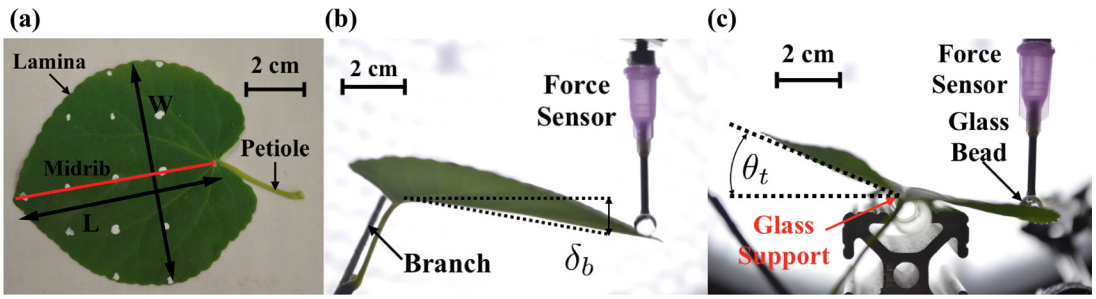

Figure 1. (a) Image of a typical Katsura leaf showing the characteristic length dimensions, lamina and the petiole. (b) Experimental setup showing how bending rigidity of the leaf (EI) is determined. (c) Experimental setup showing how torsional rigidity of the leaf (GJ) is determined.

along with external environmental factors like wind [1]. Static and dynamic response of these modes for a leaf have also been demonstrated as an equivalent response of cantilever beams [18, 21]. Yet a leaf experiencing multiple degrees of freedom like bending and torsion simultaneously in response to a raindrop impact exerting impulsive force on the leaf remains poorly studied.

In this study, we decompose the complex response of a leaf upon raindrop impact into simple single degree of freedom linear modes of bending and torsion. The 3D motion of the leaf is tracked using two high speed cameras and characteristic parameters like amplitude and frequency of each mode are measured from 3D-tracked leaf motions. This is followed by development of simple theoretical models to correlate the leaf's response to natural modes of bending and torsion. Maximum deflections observed for these modes, in the limit of small deflections, were also measured with comparison to theoretical estimates using simple angular conservation for each of the modes. We believe this study to be useful in analyzing nature's very own design, the leaf's response and in some way mimic it for energy harvesting devices [22–24]. Accordingly, we provide estimates of energy transfer to the modes of bending and torsion and their dependence on various influencing parameters. We then speak briefly about an unresolved secondary torsion mode, resembling flapping of a bird's wings, present in the complex motion. Lastly, we briefly discuss the limitations of theory used to understand the leaf's dynamic response.

Material and methods

Sample procurement

For the study, Katsura tree (*Cercidiphyllum japonicum*) leaf specimens were chosen which are deciduous trees native to China and Japan [25]. The mature leaves are heart-shaped, hydrophobic (which is a factor helpful for reducing the dependency of previous experiments on the same leaf) and approximately 7 cm long and 6 cm broad, having an aspect ratio of approximately one. The leaves tend to grow together, closely packed on branches and big mature ones from such a branch were chosen each time for the experiment. The average mass of a mature leaf ($N = 13$) is 460 ± 50 mg. For the study, Katsura trees near Gilbert street at Virginia Tech (37°14′00.3″N, 80°25′17.1″W) were selected. The primary location, Blacksburg lies in a humid climate zone and experiences an average temperature ranging from 4.5 °C to 17.3 °C annually. Definitive weather conditions like wind speed, relative humidity and annual precipitation are approximately 2 m s^{-1}, 76% and and 1000 mm, respectively [26]. For this study, seasonal variation's impact on the leaves was also inspected which will be discussed in future followup works. The summer season leaves were taken approximately from May 2018 to July 2018 while the fall season leaf samples were taken from October 2017 to November 2017. The summer leaves were observed to be fully grown dark green hydrophobic leaves while the fall leaves were yellow or brown fragile leaves with reduced hydrophobicity, based on the measured averaged contact angles, changing from 147° to 124° from summer to winter [15].

As soon as the branches were detached, the leaves were transferred to the lab and kept hydrated throughout the mechanical tests and the experiments with the help of a syringe. To prevent effect of desiccation further, all of the experiments were conducted within few hours of leaf detachment. The leaves were photographed for recording the leaf blade length L and the leaf blade width W as shown in figure 1(a), followed by mechanical tests and the drop impact experiments.

The midrib of the leaf is the thickest vein that goes from the leaf petiole end to the leaf tip and is highlighted in figure 1(a). It is also the most prominent axis of motion, and corresponds to the axis of the torsional mode referenced in our study (though torsion is localized in the petiole). To calculate the polar moment of inertia (for the torsional mode), after the impact tests, cuts were made on the leaf making slices parallel to the midrib to have at least 10–15 slices. Each slice was weighted to calculate its mass and then the product of the mass of each slice and the distance squared from the midrib was summed over all the slices to get an approximate value of the polar moment of inertia of the leaf about the midrib. The midrib also corresponds to the bending axis of a cantilever, causing

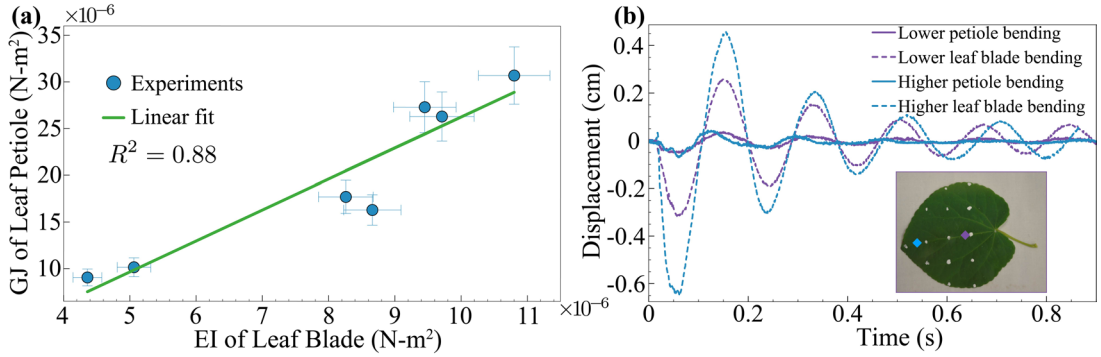

Figure 2. (a) *GJ* of petiole versus *EI* (N m^2) of leaf blade for Katsura leaf experiments. (b) Deflections for marker point near the petiole (solid line) and marker point near the leaf tip (dashed line) versus time for lower and higher impact torque scenarios. Respective impact points and their location on the leaf is shown at the bottom right.

the leaf lamina to bend on the application of a vertical force. Accordingly, a similar process for the calculation of bending moment of inertia (for the bending mode) would be to make thin strips perpendicular to the midrib and then sum up the individual moments of inertia of these strips. This process would then approximate a leaf as an equivalent cantilever with a modified moment of inertia. Unfortunately, calculating both the moments of inertia in this way simultaneously, leads to decreased ease of handling of the leaf strips and is not feasible experimentally. Hence a crude approximation of a uniform cantilever is made for the leaf for the bending mode. The effects of this approximation on the theoretical amplitude and frequency estimates for the bending mode are discussed in the future sections. Data to calculate the polar moment of inertia about the midrib has been provided in the supplementary material (stacks.iop.org/BB/15/036007/mmedia). Secondary torsion of smaller veins perpendicular to the midrib also gives rise to another mode, referenced as 'flapping' in the following section. However, due to the relatively fast time scale of this flapping motion, corresponding measurements and analysis lie in the scope of future work.

To characterize the motion of the leaf for the bending and twisting degrees of motion, we then calculate lumped values of bending (*EI*) and torsional (*GJ*) rigidity, as explained in the following sub sections. More accurate predictions using advanced beam models like Kirchoff or Cosserat beam theories with varying *EI* and *GJ* are possible, however the central idea behind this study is to show the possibility of the decomposition of the complex motion into well studied simpler degrees of freedom.

Bending test

An experimental setup shown in figure 1(b) is used to determine lumped bending rigidity (*EI*) for the leaf. The leaf petiole end attached to the branch is held in place with a clip while the tip of the leaf is displaced using a linear stage probe downwards while loading and upwards during unloading, allowing the midrib and lamina to bend during the test. The probe consists of a needle glued with a smooth glass bead at the free tip. A borosilicate glass bead of diameter 0.25 inch was used for a smooth and concentrated point of contact with the leaf. The other end of the needle is attached to a 10 g force sensor (LSB200; Futek Inc.). This entire 'probe' setup is controlled using a Velmex linear stage for the accurate vertical displacement. By displacing only the tip, no torque is applied along the midrib and only the bending mode deflection of the leaf is observed. During the loading-unloading cycle, the force exerted by the leaf is measured using the piezoelectric sensor at the tip of the linear stage probe (shown in figure 1(b)). The force experienced at the tip is correlated with the tip deflection using 1D Euler–Bernoulli beam theory [27] for cantilever tip displacement as shown in equation (1)

$$\delta = \frac{FL^3}{3EI} \tag{1}$$

where EI, δ, F and L are the cantilever bending rigidity, tip deflection of the cantilever, force applied at the tip and the length of the beam, respectively. Three loading and three unloading cycles are performed for each leaf and the slopes of the tip force versus tip deflection angle plots are used to determine the bending rigidity based on equation (1). The average value found for bending rigidity of a mature leaf ($N = 7$) is $8.0 \pm 2.4\ \mu\text{Pa} \cdot \text{m}^4$. Also, the bending shown by the petiole is found to be negligible compared to the bending shown by the leaf blade. We confirmed this fact by tracking deflections of a marker point near the petiole end and another one far away from the petiole, for lower and higher impact torque cases, as shown in figure 2(b).

Torsional test

An experimental setup shown in figure 1(c) allows us to measure the lumped torsional rigidity (*GJ*) for the leaf. The leaf midrib is gently supported on a glass rod to ensure that the leaf blade rotates freely about the midrib and that no secondary torsion (bending perpendicular to midrib) is involved. We note that this support is used only during the torsional test to restrict the bending mode, but is not used during the drop

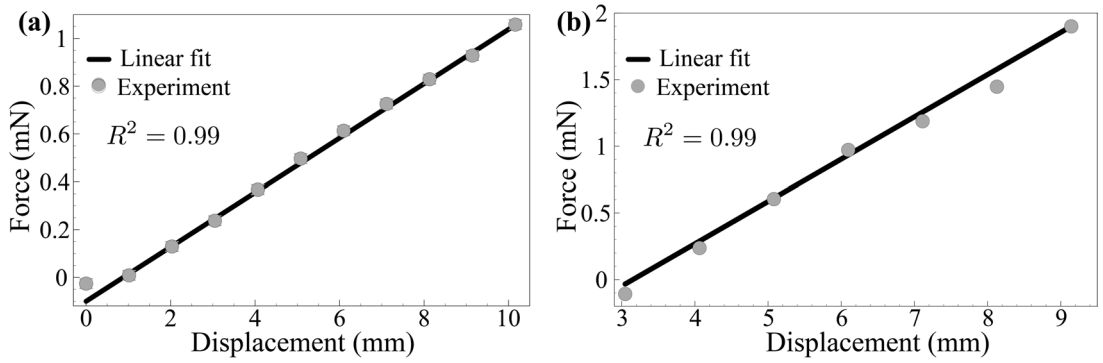

Figure 3. (a) Typical force from a force sensor versus displacement of the leaf tip, from images for a bending test. (b) Typical force from a force sensor versus displacement of the leaf edge, from images for a torsion test. The grey circles denote experimental values while the black line is the linear fit whose slope is used to calculate the bending or torsional rigidity.

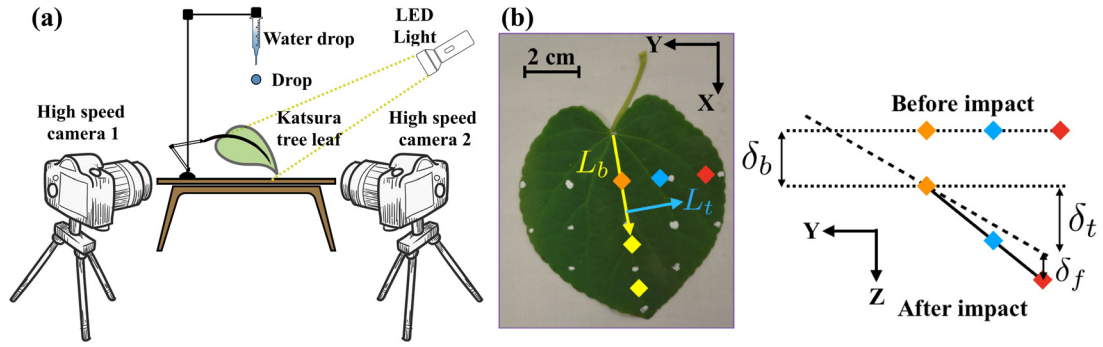

Figure 4. (a) Drop impact experimental setup showing how a raindrop being simulated through a syringe is imaged and tracked in 3D with the help of two high speed cameras. (b) Schematic showing the separation of the deflections of the different observed modes along with the variation of the impact points for torsional mode variation (red, blue and red markers) and bending mode variation (yellow markers). The deflection of white markers on the midrib consists only of bending, which is then subtracted from the net deflection of other white markers lying on the same bending moment arm (distance from petiole end) to get torsion and secondary torsion deflections. Torsional and secondary torsion are then separated by tracking displacements of markers, symmetrically opposite to the midrib. This is possible due to the fact that symmetrically opposite points have equal and opposite torsional mode deflections.

impact tests, thus avoiding any artificial constraints and allowing the leaf to exhibit a natural dynamic response. The edge of the leaf blade is displaced using a linear stage probe in the downward direction during the loading cycle and upwards during the unloading cycle. During this process, the torque exerted by the leaf is measured using the piezoelectric sensor at the tip of the linear stage probe. This torque is correlated to the angle of twist using torsional shaft theory for small displacements [28], given by

$$GJ = \frac{TL}{\theta} \tag{2}$$

where GJ, T, θ and L are the torsional rigidity, measured torque, angle of twist, and length of the leaf lamina, respectively. Typical force versus displacement plots for the piezoelectric sensor and the corresponding linear fits for bending test and torsion test are shown in figure 3 for the loading phase. Three loading and unloading cycles are performed for each leaf and the slopes of the torque versus angle of twist plots are used to determine the torsional rigidity based on equation (2). The average value found for torsional rigidity of a mature leaf ($N = 7$) is $19.6 \pm 8.6\ \mu\text{Pa} \cdot \text{m}^4$. Figure 2(a) presents the variation of GJ of the leaf petiole with EI of the midrib (and the leaf blade) for different leaf specimens, pointing to the fact that the midrib along with the leaf blade bends more than the petiole twists.

With preliminary tests to capture structural properties of the leaf, we then describe our experimental setup and technique to capture dynamics of the leaf in the next subsection.

Experimental setup and imaging

The schematic of the setup for the drop impact has been described in figure 4(a). The leaf specimen is placed at the center of the table with two high-speed Photron Mini cameras focused on it for capturing the dynamics of the 3D response of the leaf to drop impact. Also, several white markers have been placed on the leaf surface (as shown in figure 1), allowing 3D tracking of the leaf dynamics. The 2D images received from these cameras were rendered into a 3D space using the DLTdv Digitizing tool developed by Hedrick Lab at UNC, USA [29]. The two synchronized cameras record images at a speed of 2000 frames per second to capture the leaf dynamics in a highly resolved manner,

as the leaf drop response has a time period of the order of 100 ms.

To simulate raindrops, water is supplied very slowly using a syringe pump (Model no. NE-1000, Serial no. 269269) and exits through a syringe generating drops of radius ($R = 1.8 \pm 0.1$ mm) and mass ($m_d = 25 \pm 1$ mg). These drops are released from heights varying from 15 to 86 cm, resulting in impact speeds (V_d) in the range of 1.5–3.8 m s^{-1}, which is close to the lower end of the range of mid size raindrops [17]. The drop radius produced in our experiments lies in the moderate bandwidth [17, 30] of typical raindrop sizes, thus taking into account average case scenario for impact momentum which scales with the drop mass. The location of drop-impact points on a leaf has been depicted in figure 4(b) as yellow, orange, blue and red markers. For each leaf, 5–6 impact points were tested varying the distances L_b (bending moment arm: distance from petiole end) and L_t (torsional moment arm: distance from midrib) independently as shown in figure 4(b). For each impact point, 3 repeated trials were conducted to ensure statistical significance of results. As shown in figure 4(b), all the points have different L_b and L_t and hence the excitation of each mode is different for each of these points. The coordinates of the impact point are also tracked using the high speed cameras for each trial which are later used for theoretical estimates of the maximum deflection. Efforts were made to avoid the edge of the leaf during drop impact to prevent edge spillage of the drop. Due to hydrophobic nature of Katsura leaves, non wetting of the leaf for each trial is observed, resulting in independence of each trial as there were no water residues left from experimental trials. Thirteen leaves were tested, and the drop velocity was also varied for 6 of them.

All experiments were performed within 1–2 h of the removal of the leaf from the tree and the leaves were kept hydrated throughout the experiments. The experimental time scale is 2–3 orders of magnitude shorter than the time scale where desiccation shows significant changes in properties of the leaf [31]. We then begin the analysis of our results in the next section.

Experimental results

Before the analysis of our results, we discuss the primary degrees of freedom of motion possible for the leaf from a structural point of view. Most leaves have a thick vein (i.e. midrib) along the center line and symmetric blades on both sides. This symmetric leaf blade (or lamina) is wide, but does not curl, twist or shear itself significantly according to experimental observations. The thick vein can bend like a cantilever, causing the lamina to bend as well. The petiole can twist like a twisting shaft, causing rotation of the lamina with it. The lamina can also bend perpendicular to the midrib if a torque is applied about the midrib.

With these assumptions, we hypothesize that the complex motion of a leaf upon drop impact, in the limit of small deflections, can be decomposed using the superposition principle for linear systems into three different degrees of motion: bending of the midrib and lamina, twisting of the petiole accompanied by rotation of the lamina, and secondary torsion of the lamina perpendicular to the midrib. The analysis that follows and the comparison between experiments and theory supports the superposition principle as a fair assumption in our case. The bending motion represents deflection of the leaf similar to a cantilever beam in the plane of the beam, originating from the bending of the midrib. The twisting motion of the petiole accompanied by the rotation of the lamina represents the torsional mode of a shaft. The third degree of motion known as secondary torsion is also referred to as 'flapping' herein. This mode is seen only when a drop impacts close to the edge of the leaf blade, generating sufficient torque to bend the lamina, perpendicular to the midrib. Generally, we observed a leaf motion showing all these modes simultaneously in our experiments. The schematic in figure 4(b) along with the caption illustrates how we can decompose these three modes from the net displacement of the leaf by tracking a point on the midrib and points located symmetrically on opposite sides of the midrib. In this study we look into the bending and torsional degrees of motion as they have similar timescales while secondary torsion analysis falls in the scope of future studies. This is due to faster timescales of flapping leading to shortage of frames for finely resolving the motion, at the current frame rate of the cameras.

With the above hypothesis, we now characterize the individual modes observed for the leaf in the following subsection.

Characterization of response of the leaf

A single degree of freedom response can be explained as a typical response of a damped harmonic oscillator as shown in equation (3).

$$\delta(t) = \delta_0 e^{-\zeta t}\cos(\omega t + \phi) \tag{3}$$

where δ is the deflection as a function of time, δ_0 is the initial maximum deflection, ζ is the damping coefficient and ω is the angular frequency. Experimental values of the governing parameters which include vibration frequency and maximum amplitude have been obtained by curve fitting the experimental trends using `Python SciPy` library's non linear residual minimization package. A typical good fit for the bending deflection of one of the marker points on the leaf using the library can be seen in figure 5(a) for one of the cases. As shown in figure 5(a), the timescale of oscillations for bending mode is of the order of 0.1 s, and the modes decay time is of the order of 0.5–1 s (see the supplementary video). We observe that the torsional mode also has the same order of timescale. Theoretical formulations for the oscillation frequency and initial maximum displacement for both bending and twisting have been derived and compared

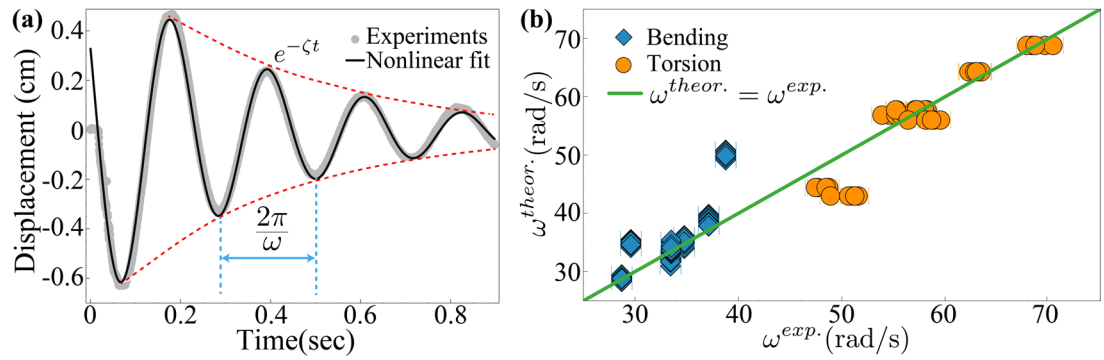

Figure 5. (a) Non-linear fit using `Python Scipy` package between experimental amplitude and theoretical amplitude versus time for a damped harmonic oscillator. The grey points denote the experimental points for the bending displacement of one of the markers points on the leaf while the black curve is the theoretical expression for a damped harmonic oscillator. The red envelope on the decaying amplitude stands for the decaying exponential curve $e^{-\zeta t}$. (b) Frequency comparison—experiments versus theory for bending and torsion. Theoretical versus experimental values are plotted with blue diamonds for bending mode data and red circles for torsional mode data. The comparison is shown with the help of the line plotted as $\omega^{theor.} = \omega^{exp.}$.

with experimental values in the following sections to support our hypothesis.

Vibration frequency: bending and torsion

Vibration frequency is calculated from the non linear curve fitting of the damped harmonic oscillator response onto the experimental curves. A theoretical estimate of the first mode of natural frequency vibrations for a cantilever [27] is given by

$$\omega_b = 3.5161\sqrt{\frac{EI}{ML^3}} \tag{4}$$

where ω_b is bending angular frequency, EI is the bending rigidity of the leaf equivalent to a cantilever, L is the length of the leaf lamina and M is the mass of the leaf. Similarly a theoretical estimate for torsional oscillation frequency can be obtained using simplified linear harmonic torsional shaft theory [28] given by

$$\omega_t = \sqrt{\frac{GJ}{LI_p}} \tag{5}$$

where ω_t is the torsional angular frequency, GJ is the torsional rigidity of the leaf equivalent to a torsional shaft, L is the length of the leaf lamina and I_p is the polar moment of inertia of the leaf about the midrib (refer to sample procurement for details of calculation of I_p). Figure 5(b) shows the comparison between the experimental and theoretical values for bending and torsional frequencies and shows agreement between the two. Frequencies are also found to be independent of the impact location or drop velocity (see data in the supplementary material), which supports the presence of a single dominant mode for the given range of parameters. Also the twisting frequency is observed to be 1.5–2 times the bending frequency implying that the leaf twists more frequently than it bends on raindrop impact; a phenomenon observed for all the specimens tested. Having confirmed that the dominant modes observed correspond to the natural modes of bending and torsion, we next obtain theoretical estimates for the maximum deflection seen in these modes using angular momentum conservation.

Maximum deflection: bending and torsion

Here, we provide theoretical estimates for maximum deflection for bending and torsion using an angular momentum conservation approach, similarly in [18, 21, 32] that focused on drop identification and dispersal mode for the bending mode. For drop impact at a considerable distance from the midrib, torsion and secondary torsion emerge as secondary modes. Accordingly, we extend the angular momentum conservation approach to the torsional mode analysis with secondary torsion analysis left as a prospect of future work.

Assuming the drop with mass m_d with an impact velocity v_d has a linear momentum of $m_d v_d$, and impacts at a distance of L_b from the petiole attachment point, angular momentum conservation about the petiole attachment point yields a theoretical estimate for maximum bending deflection as derived in equation (6).

$$\begin{aligned}&\text{Angular momentum of drop} =\\ &\text{Instantaneous angular momentum of the leaf}\\ &m_d v_d L_b \cos\theta \cong \frac{ML^2\omega_b\theta_b}{3}\\ &m_d v_d L_b \cos\theta \cong \frac{ML^2\omega_b}{3}\sin^{-1}\left(\frac{\delta_b}{L}\right)\\ &\frac{\delta_b}{L} \cong \sin\left(\frac{3m_d v_d L_b\cos\theta}{ML^2\omega_b}\right)\end{aligned} \tag{6}$$

where θ is the initial angle of inclination of the leaf from the horizon, M is the mass of the leaf, L is the length of the leaf lamina and δ_b is the bending deflection. Figure 6 shows the scaling of non-dimensional bending amplitude as a function of impact distance given by equation (6).

Figure 6 shows the comparison between theoretical and experimental non-dimensional values of bending deflection and shows a fair agreement between

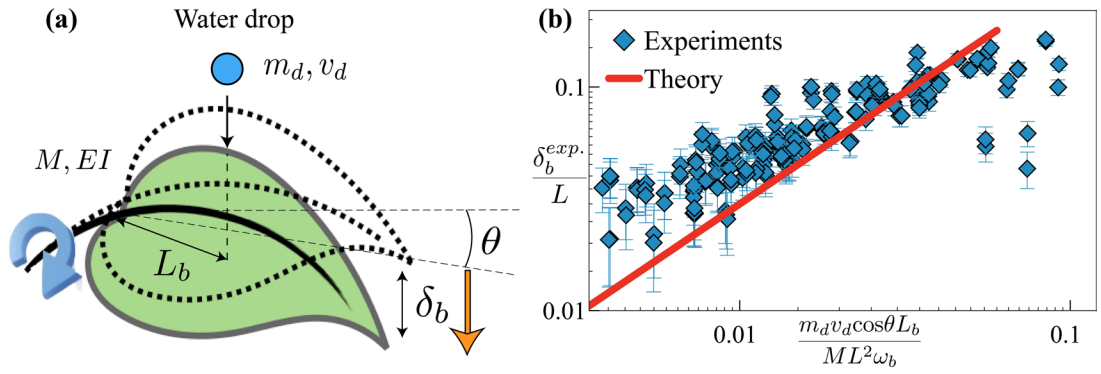

Figure 6. (a) Bending deflection schematic showing the parameters used in theoretical estimation of maximum bending deflection. (b) Non-dimensional amplitude (of the leaf tip) scaling for bending as derived from equation (6) shown as blue diamonds in the plot. Comparison between experimental and theoretical values of bending amplitude is shown versus the red line plotted as theoretical values on a log log scale.

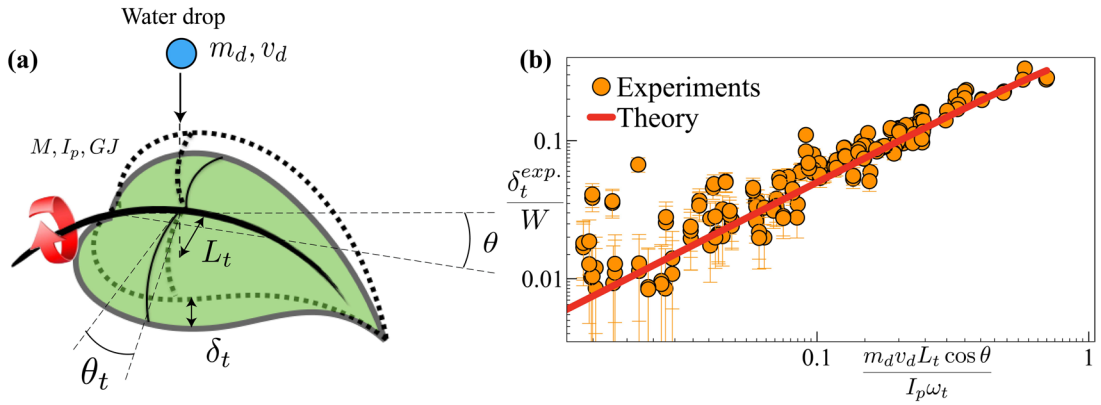

Figure 7. (a) Torsional deflection schematic showing the parameters used for calculating theoretical estimates of maximum torsional deflection. (b) Non-dimensional amplitude (of the leaf edge) scaling for torsion as derived from equation (7) shown as orange circles in the plot. Comparison between experimental and theoretical values of torsional amplitude as shown versus the red line plotted as theoretical values on a log log scale.

experiments and theory. For the case of impact locations close to the petiole (low-mid L_b), this theory under-predicts the experimental bending due to the crude assumption of a leaf as a uniform cantilever. In fact, mass in the lamina is concentrated towards the petiole than towards the leaf tip, pointing towards a lower value of bending moment of inertia for the leaf blade compared to an equivalent cantilever with the same mass and length. For higher values of L_b where the drop impacts close to the leaf tip, we observed that the drop quickly slides off from the leaf due to the drooping of the leaf near the leaf tip. This results in lesser momentum transfer than the theoretical prediction and hence an over-predicted value of bending amplitude.

Similar to bending, angular momentum conservation about the midrib yields a theoretical estimate for maximum torsional deflection as derived in equation (7).

$$\text{Angular momentum of drop} = \text{Instantaneous angular momentum of the leaf}$$

$$m_d v_d L_t \cos\theta \cong I_p \omega_t \theta_t$$

$$m_d v_d L_t \cos\theta \cong I_p \omega_t \sin^{-1}\left(\frac{2\delta_t}{W}\right)$$

$$\frac{\delta_t}{W} \cong \frac{1}{2}\sin\left(\frac{m_d v_d L_t \cos\theta}{I_p \omega_t}\right) \tag{7}$$

where I_p is the polar moment of inertia of the leaf about the midrib, W is the width of the leaf lamina and δ_t is the torsional deflection.

Figure 7 shows the scaling of non-dimensional torsional amplitude as a function of impact distance given by equation (7) and shows a strong linear dependence. Figure 7 also shows the comparison between theoretical and experimental values for torsional deflection and shows a decent agreement between experiments and theory. We also observe the theoretical estimates

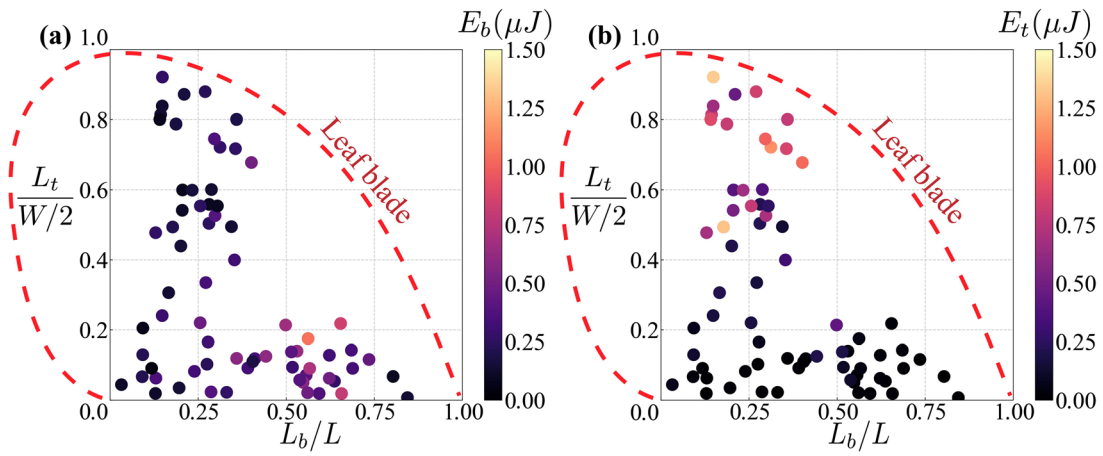

Figure 8. Variation of energy transfer to (a) bending and (b) torsional modes on raindrop impact with varying impact location on the leaf surface. L_b and L_t represent the distance from the petiole tip and the midrib, respectively. The edge of the leaf blade is illustrated by the red dotted line.

for torsion to be closer to the experimental values when compared to the ones for bending. The reason for this is the calculation of moment of inertia for bending and torsion—for torsional mode, mass variation along the leaf cross section was accounted for through the process of I_p calculation described in sample procurement section, while the same process could not be repeated for bending mode due to the process being experimentally unfeasible.

Having quantified the prominent modes with agreement between theory and experiments, we investigate the rates at which these modes decay with time through the analysis of the damping coefficients for these modes.

Damping coefficient: bending and torsion

Here, we briefly comment about the variation of damping coefficient for bending and torsion as a function of different impact locations (L_b and L_t). No significant trend was observed for the bending damping coefficient while the torsional damping coefficient showed a weak increasing trend with increasing impact location distance (L_t). It is presumably because damping originates in three different sources: dissipation in the internal leaf, attachment at the joint between the petiole and the branch, and aerodynamic drag around the leaf. Only the third one depends on the impact location (actually on the impact torque) and hence the damping coefficient has weak dependence on the impact location. The figure showing the trends for the damping coefficient can be found in the supplementary information.

With complete characterization of the bending and torsional modes as damped harmonic oscillators, we might translate insights from the modal analysis into a possible design of an energy harvester device inspired from the leaf. Accordingly, we will demonstrate one possible way of showing the proof-of-concept; analysis of the energy transfer from the raindrop to the torsional and bending modes for different impact points on the leaf, in Discussion section.

Discussion

Energy quantification: bending and torsion

After characterizing the complex motion as a superposition of bending and torsion, we provide estimates of energy transfer to these modes using theoretical models described in the previous section. Starting with bending energy which depends on the deflection of the beam and the bending rigidity, we estimate the average bending energy [18] over three cycles of oscillation using Euler–Bernoulli beam theory as shown in equation (8)

$$E_b \simeq \frac{1}{(t_f - t_0)} \int_{t_0}^{t_f} \frac{EI}{2} \frac{\delta_b(t)^2}{L^3} dt \tag{8}$$

where $t_f - t_0 = 3(2\pi)/\omega_b$ i.e. three periods of oscillations. We choose three periods of oscillations to sufficiently capture the motion before damping renders the motion unable to be resolved. Similarly the torsional energy, dependent on the angle of twist and torsional rigidity, is estimated as an averaged quantity over three cycles according to equation (9)

$$E_t \simeq \frac{1}{(t_f - t_0)} \int_{t_0}^{t_f} \frac{GJ}{2L} \frac{\delta_t(t)^2}{W^2} dt \tag{9}$$

where $t_f - t_0 = 3(2\pi)/\omega_t$ i.e. three periods of oscillation.

Figure 8 provides a functional relation of energy transfer from the drop's kinetic energy into the bending and torsional modes. In figure 8, the energy transfer to the torsional mode is higher for impact points away from the midrib (higher L_t) due to the higher torsional moment about the midrib on drop impact. Similarly, higher L_b values (farther from the petiole end) correspond to higher energy transfer to the bending mode. However the energy transfer to the bending mode peaks around midway ($L_b/L \sim 0.6$) along the midrib and drops for points near the tip of the leaf due to the drooping curvature of the leaf and edge spillage. The above analysis provides an integrated

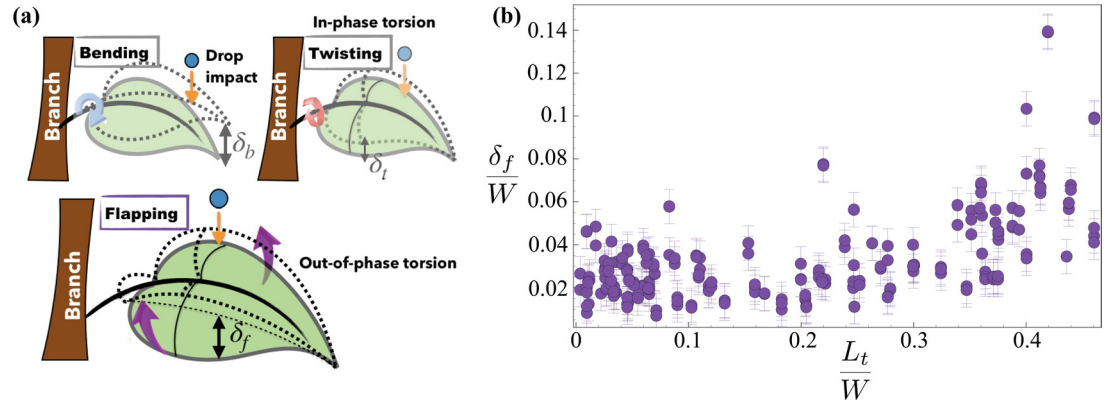

Figure 9. (a) Illustration of the different modes observed for the leaf: bending, torsion and flapping (secondary torsion) (b) Non-dimensional flapping amplitude (of the leaf edge) as a function of impact distance from the midrib shown by the purple points, showing non linear behaviour with the impact distance.

perspective of the bending and torsional modes excitation for a raindrop impact on the leaf. Previously, harnessing only the bending mode excitation energy of a piezoelectric cantilever upon raindrop impact has been studied [22–24]. We believe that a device of harnessing both the bending and torsional modes can be effective to receive more raindrop impacts with a larger area, inspired by the structure of a leaf. Our proposed hypothesis of breaking down the complex motion into simpler well studied degrees of freedom simplifies design constraints and concepts. It also provides directions to tune the concerned parameters like impact point distance from midrib or the petiole end, moment of inertia of the leaf and different rigidities to maximize total energy transfer or power output for these modes.

We now demonstrate order of magnitude calculations to illustrate the feasibility of the design of a leaf in the application of energy harvesters. During rainfall, the kinetic energy of an average size raindrop is around 1 mJ [17]. Assuming an energy conversion rate of roughly 10 percent (maximum total energy observed is $\sim$2.5 μJ in figure 8 for a raindrop of kinetic energy $\sim$25 μJ) with resonant coupling of piezoelectric sensors to the leaf, we achieve a crude estimate of transmitted power of 0.1 mW from only 40 cm^2 surface area.

In addition to certain design parameters provided by the above analysis, some factors like surface wettability, multiple drop impacts, plant response to rain and shape geometry need to be considered. The Katsura leaf used in our studies being hydrophobic, a large percentage of kinetic energy and momentum of the drop is conserved and is not transferred to the modes of consideration [18]. However, raindrop adhesion on hydrophilic leaves leads to a higher momentum and energy transfer due to the highly inelastic collision between the drop and the leaf. In our previous study on the dynamics of a cantilever beam in response to a raindrop impact [18], we showed that the transfer of energy to vibrational mode (bending) is indeed higher for the wetting surface. A mean deflection of the leaf and subsequent leaf angle change was also observed for the wetting case due to raindrop adhesion. At the same time, we should also consider the fact that a hydrophilic leaf encounters higher impact forces and torques and is more susceptible to damage compared to a hydrophobic one. Investigating the differences in the vibration modes shown by the two types of leaves and the corresponding energy harvesting potentials lies in the scope of future work. In the case of multiple drop impacts, the leaf may not achieve maximum deflection and may end up exhibiting higher nonlinear modes of vibrations. The main goal of our study was to tackle the simplest possible scenario of a single raindrop impact. Investigation of multiple raindrop impacts and higher modes of vibrations is an avenue of future study. Besides the wettability, plants response to rain [35] and the tip geometry of a surface [36] (in our case the lamina) can also influence the leaf's response to a raindrop, and thus modify the estimates our analysis provides.

We next discuss briefly the third unresolved mode called flapping (secondary torsional motion), followed by the limitations of the theoretical approach used in this study.

Flapping (secondary torsional motion) mode quantification

A third degree of motion which is the secondary torsional motion of the lamina perpendicular to the midrib (referred to flapping motion herein) was also observed in our study as shown in figure 9(a). Unfortunately the time scale of this motion was too fast to be resolved fairly with the frame rate of the cameras used and would need a much higher frame rate for detailed analysis or energy quantification of the mode. However the maximum deflections for this mode were captured and can be seen in figure 9(b), compared against the non-dimensional impact distance from the midrib. Like torsion, flapping also shows increasing dependence with the impact distance, but of a non linear nature. Characterizing this mode in detail is a part of future studies.

Limitations

We note that the linear beam theory used for the analysis of bending and torsional modes for leaf dynamics has two major assumptions; first, every cross section of the beam remains perpendicular to the neutral axis (midrib) and second, the deflection angle or the strains in the system are infinitesimal. In our study, we observe that most of the δ_b/L and δ_t/W values lie in the range of 0.01–0.1, where the deflection angles can be considered fairly small; thus the linear beam theories provide fair enough theoretical estimates for deflection and frequencies. We believe for higher drop impact speeds or impact torques, the deflections would not be infinitesimal rendering linear beam theories inadequate. Besides modes like shearing and uni-axial extension along with out of plane 'warping' may also be excited rendering the linear superposition principle inadequate. In such high impact torque regimes, we recommend the use of advanced beam theories like extension of Euler–Bernoulli beam theory for large deflections [33], Timoshenko beam theory [27] which captures bending and shear or the Cosserat beam theory [34] which captures bending, twist, shear and stretch at the same time for large deflections.

Conclusions

We characterized the complex response of a leaf to raindrop impact into three simple modes of bending, torsion and flapping (secondary torsion) hypothesizing that the principle of superposition works for the given scenario in the range of small displacements. Extracting the bending and torsional rigidity of a leaf equivalent to a cantilever and torsional shaft, we showed that the leaf does indeed vibrate in fundamental natural modes of bending and torsion, equivalent to a damped harmonic oscillator. Using simplified angular momentum conservation about the lamina end and midrib, we obtained theoretical estimates for the maximum deflections, which show decent agreement for torsion and a fair one for bending; which was justified with a number of reasons. Finally we demonstrated the energy transfer to these modes depending on the impact location on the leaf to provide a rationale for the design of energy harvesting devices inspired from nature's common design, i.e. a leaf. Finally, we summarized with a brief account of secondary torsion or flapping and the limitations of the linear beam theory in capturing the dynamics of the leaf. Questions like seasonal variation of these modes if present, multiple raindrop impacts, and the damage consideration of the leaf due to these modes remain unanswered in the present and lie in the scope of future work.

Acknowledgments

This research was supported by the National Science Foundation Grant CBET-1604424. The authors acknowledge the initial contribution by Paul Dewost.

Author contributions statement

SJ conceived the experiments, YB, EE, KB, and SJ conducted the experiments, YB and KB analysed the results. All authors reviewed the manuscript.

Additional information

Competing interests: The authors declare no competing interests.

ORCID iDs

Sunghwan Jung https://orcid.org/0000-0002-1420-7921

References

[1] Louf J F, Nelson L, Kang H, Song P N, Zehnbauer T and Jung S 2018 How wind drives the correlation between leaf shape and mechanical properties *Sci. Rep.* **8** 16314
[2] Kim S, Park H, Gruszewski H A, Schmale D G and Jung S 2019 Vortex-induced dispersal of a plant pathogen by raindrop impact *Proc. Natl Acad. Sci.* **116** 4917–22
[3] Amador G J, Yamada Y, McCurley M and Hu D L 2013 Splash-cup plants accelerate raindrops to disperse seeds *J. R. Soc. Interface* **10** 20120880
[4] Braam J 2005 In touch: plant responses to mechanical stimuli *New Phytologist* **165** 373–89
[5] Mann J A, Tatchell G M, Dupuch M J, Harrington R, Clark S J and McCartney H A 1995 Movement of apterous *Sitobion avenae* (homoptera: Aphididae) in response to leaf disturbances caused by wind and rain *Ann. Appl. Biol.* **126** 417–27
[6] De Langre E 2008 Effects of wind on plants *Annu. Rev. Fluid Mech.* **40** 141–68
[7] Tadrist L, Saudreau M and De Langre E 2014 Wind and gravity mechanical effects on leaf inclination angles *J. Theor. Biol.* **341** 9–16
[8] Warren J 2015 Is wind-mediated passive leaf movement an effective form of herbivore defence? *Plant Ecol. Evol.* **148** 52–6
[9] Blossey R 2003 Self-cleaning surfaces—virtual realities *Nat. Mater.* **2** 301
[10] Otten A and Herminghaus S 2004 How plants keep dry: a physicist's point of view *Langmuir* **20** 2405–8
[11] Eadie L and Ghosh T K 2011 Biomimicry in textiles: past, present and potential. An overview *J. R. Soc. Interface* **8** 761–75
[12] Cheng Q, Li M, Zheng Y, Su B, Wang S and Jiang L 2011 Janus interface materials: superhydrophobic air/solid interface and superoleophobic water/solid interface inspired by a lotus leaf *Soft Matter* **7** 5948–51
[13] Bechert D, Bruse M, Hage W and Meyer R 2000 Fluid mechanics of biological surfaces and their technological application *Naturwissenschaften* **87** 157–71
[14] Barthlott W and Neinhuis C 1997 Purity of the sacred lotus, or escape from contamination in biological surfaces *Planta* **202** 1–8
[15] Kang H, Graybill P M, Fleetwood S, Boreyko J B and Jung S 2018 Seasonal changes in morphology govern wettability of katsura leaves *PLoS One* **13** e0202900
[16] Klamerus-Iwan A and Błońska E 2018 Canopy storage capacity and wettability of leaves and needles: the effect of water temperature changes *J. Hydrol.* **559** 534–40
[17] Soto D, De Lariviere A B, Boutillon X, Clanet C and Quéré D 2014 The force of impacting rain *Soft Matter* **10** 4929–34
[18] Gart S, Mates J E, Megaridis C M and Jung S 2015 Droplet impacting a cantilever: a leaf-raindrop system *Phys. Rev. Appl.* **3** 044019
[19] Hassani M, Mureithi N W and Gosselin F P 2016 Large coupled bending and torsional deformation of an elastic rod subjected to fluid flow *J. Fluids Struct.* **62** 367–83
[20] Vogel S 1992 Twist-to-bend ratios and cross-sectional shapes of petioles and stems *J. Exp. Bot.* **43** 1527–32

[21] Niklas K J 1999 A mechanical perspective on foliage leaf form and function *New Phytologist* **143** 19–31
[22] Guigon R, Chaillout J J, Jager T and Despesse G 2008 Harvesting raindrop energy: experimental study *Smart Mater. Struct.* **17** 015039
[23] Guigon R, Chaillout J J, Jager T and Despesse G 2008 Harvesting raindrop energy: theory *Smart Mater. Struct.* **17** 015038
[24] Biswas P, Uddin M, Islam M, Sarkar M, Desa V, Khan M and Huq A 2009 Harnessing raindrop energy in Bangladesh *Proc. Int. Conf. on Mechanical Engineering*
[25] Chien H 1992 *Cercidiphyllum japonicum Sieb. et Zucc.* China Plant Red Data Book: Rare and Endangered Plants ed L Fu and J Jin (New York: Science Press) pp 212–3
[26] 2018 Blacksburg weather forecast office: annual climate report of Blacksburg (https://w2.weather.gov/climate/index.php?wfo=rnk)
[27] Timoshenko S 1983 *History of Strength of Materials: with a Brief Account of the History of Theory of Elasticity and Theory of Structures* (New York: Courier Corporation)
[28] Seaburg P A and Carter C J 1997 Torsional analysis of structural steel members *Technical Report (Steel Design Guide Series No. 9)* AISC
[29] Hedrick T L 2008 Software techniques for two-and three-dimensional kinematic measurements of biological and biomimetic systems *Bioinspiration Biomimetics* **3** 034001
[30] Villermaux E and Bossa B 2009 Single-drop fragmentation determines size distribution of raindrops *Nat. Phys.* **5** 697
[31] Dosmann M S, Graves W R and Iles J K 1999 Drought avoidance in katsura by drought-induced leaf abscission and rapid refoliation *HortScience* **34** 871–4
[32] Gilet T and Bourouiba L 2015 Fluid fragmentation shapes rain-induced foliar disease transmission *J. R. Soc. Interface* **12** 20141092
[33] Reddy J N 2014 *An Introduction to Nonlinear Finite Element Analysis: with Applications to Heat Transfer, Fluid Mechanics, and Solid Mechanics* (Oxford: Oxford University Press)
[34] Rubin M B 2000 *Cosserat Theories: Shells, Rods and Points* vol 79 (Berlin: Springer)
[35] Moerkercke A V *et al* 2019 A MYC2/MYC3/MYC4-dependent transcription factor network regulates water spray-responsive gene expression and jasmonate levels *Proc. Natl Acad. Sci.* **116** 23345–56
[36] Cheng Z, Gao J and Jiang L 2010 Tip geometry controls adhesive states of superhydrophobic surfaces *Langmuir* **26** 8233–8